Journal of Thermal Engineering
Web page info: https://jten.yildiz.edu.tr
DOI: 10.14744/thermal.0001024

Research Article

Performance assessment of solar based trigeneration system using organic rankine cycle and ejector refrigeration system

Yunis KHAN[1,*], K.K. SIVAKUMAR[2], P. M. G. Bashir ASDAQUE[3], D. APPARAO[4], Rajesh KUMAR[5], Kumar GAURAV[5], Lalit BATRA[6]

[1]*Department of Mechanical Engineering, Indian Institute of Technology (ISM), 826004, Jharkhand, India*
[2]*School of Liberal Arts and Sciences, Babu Mohan University, 517102, Andhra Pradesh, India,*
[3]*Department of Mechanical Engineering, Dayananda Sagar University, Banglore, India*
[4]*Department of Mechanical Engineering, Aditya Institute of Technology and Management, 532201, Andhra Pradesh, India*
[5]*Department of Mechanical Engineering, Sandip University, Bihar, 847235, India*
[6]*Department of Applied Sciences (Mechanical), Bharati Vidyapeeth College of Engineering, New Delhi, 110063, India*

ARTICLE INFO

Article history
Received: 24 September 2024
Accepted: 12 May 2025

Keywords:
Exergy; Exergoenvironmental Impact; Solar Power Tower; Helium Brayton Cycle; Ejector Refrigeration System

ABSTRACT

In this study, a novel trigeneration system was developed to harness high-temperature solar energy from a solar power tower, enabling simultaneous generation of power, heating, and cooling effects. The system comprises a Brayton cycle utilizing helium as the working fluid, complemented by an organic Rankine cycle with an ejector refrigeration system to recover waste heat from the Brayton cycle. Energy, exergy, and exergoenvironmental analyses were conducted on the proposed system using engineering equation solver software. The heating and cooling effects were generated at 50°C and 10°C, respectively for building applications such as hospitals and hostels. The proposed plant was obtained the exergy and energy efficiencies of 25.12% and 23.30%, respectively. Additionally, cooling loads, heating loads and power output were obtained as 8.25 kW, 60.52 kW and 14998 kW, respectively. Moreover, the exergoenvironmental impact coefficient has a high value of 4.028 due to the lower exergy efficiency of the plant. The exergetic stability factor was determined to be 0.2483.

Cite this article as: Khan Y, Sivakumar KK, Asdaque PMGB, Apparao D, Kumar R, Gaurav K, Batra L. Performance assessment of solar based trigeneration system using organic rankine cycle and ejector refrigeration system. J Ther Eng 2026;12(1):1−15.

INTRODUCTION

By 2040, the global energy demand will have increased by at least 50%. Future security and sustainability depend on the production of carbon-free energy [1, 2]. The remarkable concentrated solar power (CSP) system can provide the requirement for safe and reliable electricity [3]. The CSP is using nowadays for high temperature power generation. Critical pressure of supercritical sCO2 cycle is higher than that of any other cycles [4, 5]. The sCO_2 is useful since it

***Corresponding author.**
*E-mail address: yuniskhan21@gmail.com

This paper was recommended for publication in revised form by Editor-in Chief Ahmet Selim Dalkilic

is chemically stable, non-flammable, environmentally friendly, inexpensive, and non-toxic. The CO2 cycles have increased interest recently due to their better performance at high-temperature waste recovery, also it uses the compact machinery due high density as critical points [6].

The conventional Rankine cycles and closed Brayton cycle could be employed in SPT facilities to convert heat into electricity based on their heat source temperature. Due to its benefits, including its compact size and efficient operation, the sCO2 Brayton cycle has gained a lot of attention lately [7-9]. The advantages and precise sCO_2 system layouts for use in nuclear and solar power plants were published by Guo et al. [10]. Also, they discussed the key aspects of the application and key issues related to the sCO2 cycles technology. Gkountas et al. [11] investigated the Al2O3 nanofluid for improving heat transfer led to a 0.9% decrease in heat exchanger length and a 14% decrease in pressure drop as a result in the sCO_2 system. Chai and Tassuo [12] did detailed examination of the heat exchanger parameters used in the helium and sCO2 Brayton cycles. They found that stainless steel is the ideal material that can work up to 650°C of temperature, whereas alloys based on nickel are suggested for use at greater temperatures. Also recently, Qin et al. [13] studied the system of the recompression sCO2 cycle Brayton cycle combined with the transcritical CO_2 (tCO_2) refrigeration system for recovering waste heat from the marine turbine for simultaneous refrigeration and power production. The observed COP (coefficient of performance) and levelized cost of electricity (LCOE) and waste heat recovery efficiency of the proposed system were 3.059, 18.348 $/kWh, and 0.651, respectively. At the period also Khatoon and Kim [14] proposed the sCO2 Brayton cycle operated by the SPT system with thermal storage. Proposed system fluctuation energy efficiency was found to be 39% to 45%. Using the regeneration and recompression cycles, the calculated mean net power output is 37.17 MW and 39.04 MW, respectively. Khan and Mishra [15] looked into another sCO2 technique for SPT plants. They observed a sCO2 recompression cycle with intercooling at the main compressor coupled with ORC, and their results for energy and exergy efficiency at the 0.95 kW/m2 of DNI (direct normal irradiation) were 54.42% and 80.39%, respectively. The most effective waste recovery was achieved when the sCO_2 cycle was combined with an ORC or another bottoming cycle.

In addition to the sCO2, helium is a hot topic of research as the working fluid in the Brayton cycle nowadays due to helium working better than CO2 at elevated temperatures, and Brayton cycles with helium can achieve more efficiency than that of the CO2 Brayton cycles, according to previous studies [28, 29]. To fulfil the above statement recently, a combined HBC (helium Brayton cycle) and cascaded vapor compression-absorption refrigeration system based on SPT was presented by Khan and Mishra [9] for the combined low-temperature cooling, heating, and power generation. The thermal, exergy efficiency, and power output of the recommended plant were observed to be 39.53%, 28.82%, and 14,865 kW, respectively. However, observed coefficients of performance (COP) for heating and cooling were 1.539 and 1.5391 at 80°C and -20°C of the generator and evaporator temperatures, respectively. Zhou et al. [20] employed the vapor absorption cycle as the bottoming cycle to cool the HBC's inlet while using the HBC as the topping cycle. They found optimized exergy efficiency outperformed the basic cycle by 14.5%. Bi and Lu [18] suggested a hydrogen liquefaction method based on HBC. They arrived at the conclusion that the proposed technique could liquefy gas and make hydrogen with less energy. Li et al. [19] designed three regenerative HBCs to enhance the efficiency of SPT operating at ultra-high temperatures (>1300°C). These cycles included a single-reheat cycle with intercooling, a double-reheat cycle with intercooling, and one with intercooling. After conducting a study, they concluded that when a temperature differential higher than 1000°C is required, only the cycle with intercooling could satisfy the criteria.

Many research studies have been conducted in the area of trigeneration systems with ejector refrigeration systems (ERS). For example, Wang et al. [21] looked into a trigeneration plant that uses flat plate collectors to absorb solar energy to power an ejector and an ORC. This system has an extra auxiliary heat source in addition to a storage system. Mishra et al. [22] proposed a combined cycle for power generation and cooling with dual ERS, simultaneously. They did exergoeconomic analysis on it. They concluded that the exergy and energy efficiency were improved by 6% and 11%, respectively, as compared to the basic system. They also found that the cost of the system was decreased by 11.7% as compared to a simple ERS. Ogaili et al. [23] developed a trigeneration system, which uses a zeotropic mixture as the working fluid and ERS powered by solar heat, designed to generate power, heat, and cool simultaneously. They came to the conclusion that the plant was assigned 4062.6 kW of power for heating and cooling, 1616.4 kW for cooling, and 51.52 kW for both. Saladi et al. [24] conducted an exergoeconomic, thermodynamic, and exergoenvironmental analysis of a solid oxide-based trigeneration system, incorporating an ERS for cooling. Moreover, the average environmental impact per unit of energy output was calculated to be 2877 mPts/GJ.

The literature given above suggests that not much study has been done on the Brayton cycle, that helium is utilized as the working fluid, and that a concentrated solar power tower system serves as the heat source for the electricity production. In most previous investigations, the ORC was used as the bottoming cycle, such as [25, 26]. In this study, however, a bottoming system that integrated an ejector system with an ORC was utilized to generate additional electricity and provide simultaneous heating and cooling benefits for buildings like hospitals and hostels. For the first time, ORC-ERS was employed in this study as the bottoming cycle for the HBC system run by the SPT plant. This statement defines the present research novelty. The goals of the current investigation are

- To develop an ejector refrigeration-based tri-generation system for the SPT plant that would generate cooling and heating effects at 10°C and 50°C, respectively, for use in buildings like hospitals and hostels.
- To investigate the performance of the proposed trigeneration system based on exergy, energy, and exergoenvironmental (3E) analysis.
- To use parametric analysis to look into how the various SPT system key factors and combined cycle affect the plant's performance.
- To compare the suggested novel trigeneration system's performance with that of earlier comparable conventional systems.

SYSTEM DESCRIPTION

The proposed system schematic diagram is presented in Figure 1. The SPT sub-system is used as the heat source to drive the proposed combined system. Air has been used as the heat transfer fluid (HTF) due to its free availability. The HBC takes heat from the SPT subsystem via the internal heat exchanger (IHE). Helium, as opposed to sCO_2, is the working fluid in the topping cycle. A waste heat recovery unit (WHRU) is utilized to transfer residual heat to the bottoming combined ORC-ERS. The flow direction of the working fluid can be elucidated by considering that heated, high-temperature helium enters the helium turbine (HT) (from states 4 through 5) via the IHE, where it expands after receiving heat from the SPT system. Subsequently, the expanded stream proceeds to the recuperator (from states 5 to 6), where a cooler stream absorbs the heat from the expanded stream. Finally, any remaining heat is absorbed by the ORC-ERS at the bottom through the WHRU (from states 6 to 7). The helium compressor (HC) was used to further compress it (states 1 to 2). The cold stream of helium travels to the IHE after passing through the HTR (states 2 to 3). In contrast

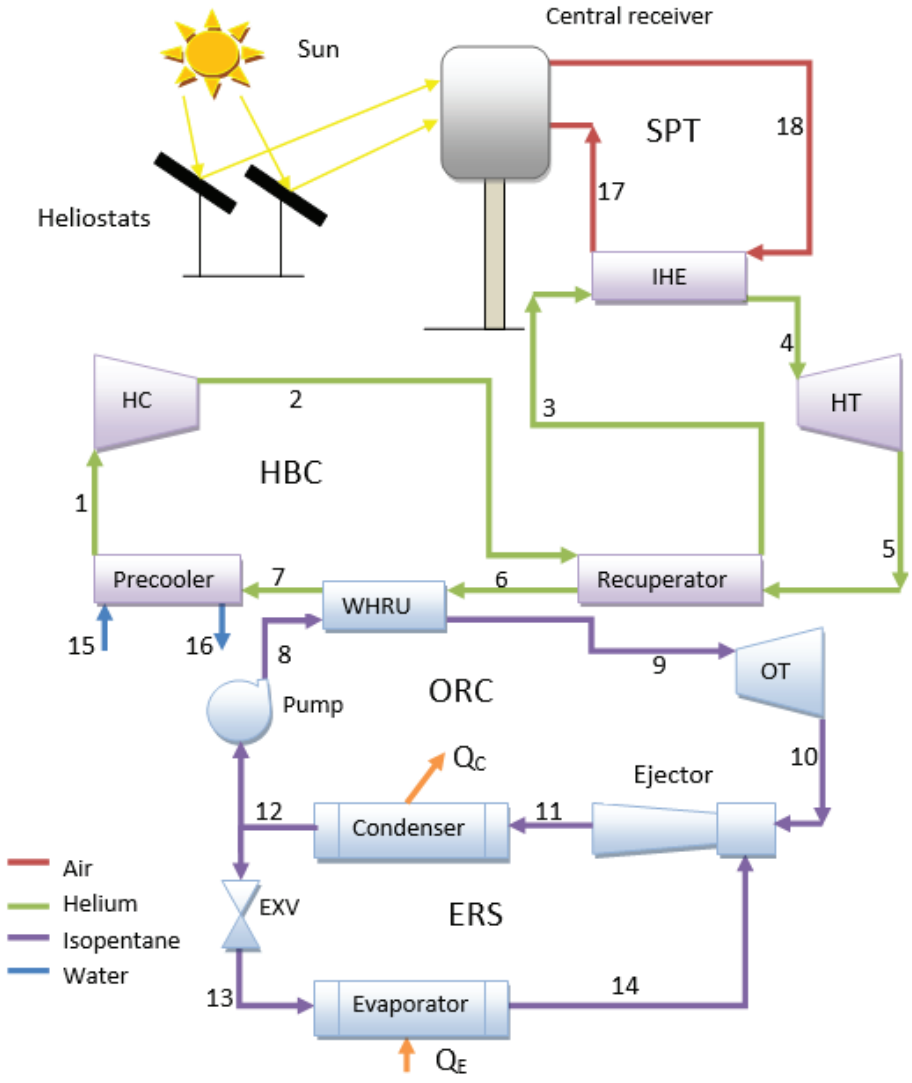

Figure 1. Diagram of the proposed plant.

to the topping cycle, the bottoming combined ORC-ERS is heated through the WHRU. Through the bottoming cycle, cooling and heating from the condenser were obtained to fulfil industrial design. The ORC-ERS system under study uses isopentane as its working fluid. This response should be trusted because isopentane has been studied in similar setups in other research studies [26, 27]. This study is particularly noteworthy for its choice of isopentane, which has not previously been examined in the context of ORC-ERS. The critical pressure and temperature of the anhydrous fluid isopentane are 187.2°C and 3380 kPa, respectively. This fluid is classified as A3 ASHRAE safe, possesses a low GWP of 20, and has almost zero ODP [25–27].

PERFORMANCE EVALUATION

Thermodynamic Evaluation

The following assumption was made (1) each component works in a steady state with one-dimensional flow. (2) The pressure loss of the components is assumed to be as indicated in Table 1. (3) Kinetic and potential energy are disregard (4) Turbine, pump, and compressor isentropic efficiencies are assumed and reported in Table 1. (5) Saturated liquid condition is considered at pump inlet. (6) The blower or compressor is not shown in the SPT circuit because in the thermodynamic analysis it makes negligible changes [9, 20].

Table 1. Simulation data for base case

Parameter	Value	Reference
SPT		
Receiver efficiency (η_{rec})	0.75	[20]
Aperture area of receiver (A_{rec})	68.1 m^2	[16]
Efficiency of heliostat field (η_{field})	0.6428	[16]
Each heliostat area (A_{hel})	9.45 × 12.84 m^2	[16,25]
Number of heliostat (N_{hel})	624	[16]
Solar irradiation (DNI)	850 W/m^2	[25]
HBC-ORC-ERS		
HT inlet temperature (T_4)	800 °C	[16]
Isentropic efficiency of HC (η_{HC})	0.89	[16]
HC inlet pressure (P_1)	2500 kPa	[16]
Effectiveness of heat exchanger (ε)	0.95	[30]
Isentropic efficiency of HT (η_{HT})	0.90	[9,20]
OT Isentropic efficiency (η_{OT})	0.8	[16]
Maximum temperature of ORC (T_8)	197.2 °C	[16]
Condenser pinch	5 °C	[16]
WHRU pinch	10 °C	[16,25]
Sun apparent temperature (T_{Sun})	4500 K	[30]
Ambient temperature (T_o)	25 °C	[30]
Atmospheric pressure (P_o)	101.3 kPa	[30]
Mixing efficiency	0.85	[31]
Nozzle efficiency	0.9	[31]
Diffuser efficiency	0.95	[31]

For the purpose of thermodynamic analysis, the entire system is divided into three subsystems: the solar subsystem, the HBC, and the ORC-ERS. Considering each components as the thermodynamic system then these are simulated using the computer program engineering equation solver (EES). Using the control volume approach, the equation for the energy and exergy balance equation in steady state conditions is given as:

$$\dot{Q}_{CV} - \dot{W}_{CV} + \sum(\dot{m}_i h_i) - \sum(\dot{m}_e h_e) = 0 \quad (1)$$

$$\dot{ED} = \dot{EX}_{in} - \dot{EX}_{out} \quad (2)$$

Where, $\dot{E}X_{in}$ and $\dot{E}X_{out}$, represent the exergy inlet and outlet to control volume, respectively. The work and heat flow from the control volume are denoted by $\dot{W}_{CV}$ and $\dot{Q}_{CV}$ respectively. After neglecting potential and kinetic energy and chemical exergy, the physical flow exergy can be expressed as;

$$\dot{EX}_j = \dot{m}\cdot[(h_j - h_0) - T_0(s_j - s_0)] \quad (3)$$

Some amount of the heat is rejected to atmosphere because of the temperature difference between heliostats and the environment. The remaining solar heat is received by the receiver [16, 25];

$$\dot{Q}_{rec,in} = \eta_{field}\cdot\dot{Q}_{Sun} = \eta_{field}\cdot DNI \cdot A_{hel}\cdot N_{hel} \quad (4)$$

Where, heliostat field efficiency η_{field} is expressed as [16]:

$$\eta_{field} = \eta_{cos}\cdot\eta_{s\&b}\cdot\eta_{int}\cdot\eta_{att}\cdot\eta_{ref} \quad (5)$$

Where, η_{ref}, η_{int}, $\eta_{s\&b}$, η_{cos} and η_{att}, are represents heliostats reflectivity, interception efficiency, shading and blocking, cosine effect efficiency, atmospheric attenuation efficiency and respectively.

The calculations of these efficacies are not scope of this study and its true values were taken from existing solar power plant [16]. Receiver efficiency and heat absorbed by receiver both are stated as [30]:

$$\eta_{rec} = \frac{\dot{Q}_{rec,net}}{\dot{Q}_{rec,in}} \quad (6)$$

$$\dot{Q}_{rec,in} = \dot{Q}_{rec,net} + \dot{Q}_{rec,loss} = \dot{m}_{air}(h_{18} - h_{17}) + \dot{Q}_{rec,loss} \quad (7)$$

Where, $\dot{Q}_{rec,loss}$ is the heat lost to the environment due to conduction, convention and radiation heat loss.

The modelling equations of the each components are listed in Table 2. The energy and exergy efficiency of the proposed plant are expressed as [30, 31]:

$$\eta_{en} = \frac{W_{net}+Q_E+Q_C}{\dot{Q}_{Sun}} \quad (8)$$

$$\eta_{ex} = \frac{\dot{W}_{net}+\dot{Q}_E\cdot\left(1-\frac{T_0}{T_E}\right)+\dot{Q}_C\cdot\left(1-\frac{T_0}{T_C}\right)}{\dot{Q}_{Sun}\cdot\left(1-\frac{T_0}{T_{Sun}}\right)} \quad (9)$$

Where, T_{Sun} represents the apparent sun temperature used as the exergy calculation [30]. However, $\dot{W}_{net}$ of the plant is expressed as:

$$\dot{W}_{net} = \dot{W}_{HT} - \dot{W}_{HC} + \dot{W}_{OT} - \dot{W}_{pump} \quad (10)$$

Exergoenvironmental Analysis

Examining the sustainability of the power system now requires an investigation into its environmental impact alongside thermal analysis. Only thermodynamic analyses of the energy generation system is not sufficient. Therefore, environmental analysis along with the exergy is also needed which estimate sustainability. The effect of exergy efficiency and exergy destruction rate on the environment is what determines the exergoenvironmental analysis. Utilizing sources [5], the following exergoenvironmental performance metrics have been examined and discussed. The exergoenvironmental impact factor (f_{ei}) has been determined to investigate the environmental impacts. This also show how to mitigate environmental hazards by

Table 2. Modeling equations for each component

Components	Energy balance equations	Exergy balance equations
Heliostat field	$\dot{Q}_{rec,in} = \eta_{field}\cdot DNI \cdot A_{hel}\cdot N_{hel}$	$\dot{Q}_{Sun}\cdot\left(1-\frac{T_0}{T_{ref,Sun}}\right) = \dot{Q}_{rec,in}\cdot\left(1-\frac{T_0}{T_{ref,hel}}\right)+\dot{E}D_{hel}$
Receiver	$\dot{Q}_{rec,in} = \dot{m}_{air}(h_{18}-h_{17})+\dot{Q}_{rec,loss}$	$\dot{E}X_{17}+\dot{Q}_{rec,in}\cdot\left(1-\frac{T_0}{T_{ref,hel}}\right) = \dot{E}X_{18}+\dot{Q}_{rec,loss}\cdot\left(1-\frac{T_0}{T_{rec}}\right)+\dot{E}D_{rec}$
IHE	$\dot{Q}_{IHE} = \dot{m}_{air}\cdot(h_{18}-h_{17})+\dot{m}_{He}\cdot(h_4-h_3)$	$\dot{E}X_{16}-\dot{E}X_{17} = \dot{E}X_4-\dot{E}X_3+\dot{E}D_{IHE}$
Helium turbine	$\dot{W}_{HT} = \dot{m}_{He}\cdot(h_4-h_5)$ $\eta_{HT} = \frac{(h_4-h_5)}{(h_4-h_{5s})}$	$\dot{E}X_4 = \dot{E}X_5+\dot{W}_{HT}+\dot{E}D_{HT}$
Helium compressor	$\dot{W}_{HC} = \dot{m}_{He}\cdot(h_2-h_1)$ $\eta_{HC} = \frac{(h_{2s}-h_1)}{(h_2-h_1)}$	$\dot{E}X_1 = \dot{E}X_2-\dot{W}_{HC}+\dot{E}D_{HC}$
Recuperator	$(h_3-h_2) = (h_5-h_6)$ $\varepsilon_{Recuperator} = \frac{(T_3-T_2)}{(T_5-T_2)}$	$\dot{E}X_5-\dot{E}X_6 = \dot{E}X_3-\dot{E}X_2+\dot{E}D_{Recuperator}$
WHRU	$\dot{m}_{He}\cdot(h_6-h_7) = \dot{m}_g\cdot(h_9-h_8)$	$\dot{E}X_6-\dot{E}X_7 = \dot{E}X_9-\dot{E}X_8+\dot{E}D_{WHRU}$
Precooler	$\dot{m}_{He}\cdot(h_7-h_1) = \dot{m}_{water}\cdot(h_{16}-h_{15})$	$\dot{E}X_7-\dot{E}X_1 = \dot{E}X_{16}-\dot{E}X_{15}+\dot{E}D_{Preooler}$
Condenser	$\dot{Q}_C = \dot{m}_c(h_{11}-h_{12})$	$\dot{E}X_{11}-\dot{E}X_{12} = \dot{Q}_C\cdot\left(1-\frac{T_0}{T_C}\right)+\dot{E}D_C$
ORC turbine	$\dot{W}_{OT} = \dot{m}_g(h_9-h_{10})$ $\eta_{OT} = \frac{(h_9-h_{10})}{(h_9-h_{10s})}$	$\dot{E}X_9 = \dot{E}X_{10}+\dot{W}_{OT}+\dot{E}D_{OT}$
Pump	$\dot{W}_P = \dot{m}_g(h_8-h_{12})$ $\eta_P = \frac{(h_{8s}-h_{12})}{(h_8-h_{12})}$	$\dot{E}X_{12} = \dot{E}X_8-\dot{W}_P+\dot{E}D_P$
Expansion valve	$h_{12} = h_{13}$	$\dot{E}X_{12}-\dot{E}X_{13} = \dot{E}D_{EXV}$
Evaporator	$\dot{Q}_E = \dot{m}_c(h_{14}-h_{13})$	$\dot{E}X_{13}-\dot{E}X_{14} = \dot{Q}_E\cdot\left(1-\frac{T_0}{T_C}\right)+\dot{E}D_E$
Ejector	$\dot{m}_c\cdot h_{11} = \dot{m}_g\cdot h_{10}+\dot{m}_e\cdot h_{14}$	$\dot{E}X_{10}+\dot{E}X_{14} = \dot{E}X_{11}+\dot{E}D_{ejector}$

minimizing irreversibilities. Its definition is provided as the ratio of total exergy destroyed to total exergy available at the system's input [5]:

$$f_{ei} = \frac{\dot{E}D_{total}}{\dot{E}X_{Sun}} \quad (11)$$

The exergoenvironmental impact coefficient (C_{ei}), which is the inverse of exergy efficiency, is highly commended for the system under study due to its low value. Its value of '1' indicates that the system under investigation is in an optimal state and is therefore good. This can be explained mathematically as:

$$C_{ei} = \frac{1}{\eta_{ex}} \quad (12)$$

A system's environmental impact is assessed using the exergoenvironmental impact index. Performance of the system improves as the exergoenvironmental effect index (θ_{ei}) value decreases.

$$\theta_{ei} = C_{ei} \cdot f_{ei} \quad (13)$$

Exergy stability factor (f_{es}) should have its ideal value 'one' or approaching to 'one'. Therefore, system performed better on exergoenvironmental point of view. It can be represented as:

$$f_{es} = \frac{\dot{E}X_{out}}{\dot{E}X_{out} + \dot{E}D_{total}} \quad (14)$$

The exergoenvironmental impact improvement (θ_{eii}) is used to evaluate how relevant the system is to environmental conditions. A larger value of this parameter is regarded to be better for the environment than the exergoenvironmental impact index. It can be said to be:

$$\theta_{eii} = \frac{1}{\theta_{ei}} \quad (15)$$

The exergoenvironmental impact improvement and exergetic stability factor make up the exergetic sustainability index (θ_{est}). A higher value for the energetic sustainability index is advantageous to the system. The system under examination is bad for the environment if it is lower. It can be stated mathematically as;

$$\theta_{est} = \theta_{eii} \cdot f_{es} \quad (16)$$

MODELING VALIDATION

The proposed system was validated with the previous studies. HBC was validated with the study of Zhou et al. [20] as shown in Figure 2. Results show the accuracy of the present model with literature. The bottoming ORC-ERS is validated using research data from Dai et al. [35] at baseline conditions. Various factors, including enthalpies and the heat and work interactions, are compared between the findings of Dai et al. [35]. The maximum discrepancy found was 1.5%, a small percentage indicating high accuracy, according to the comparison data in Table 3.

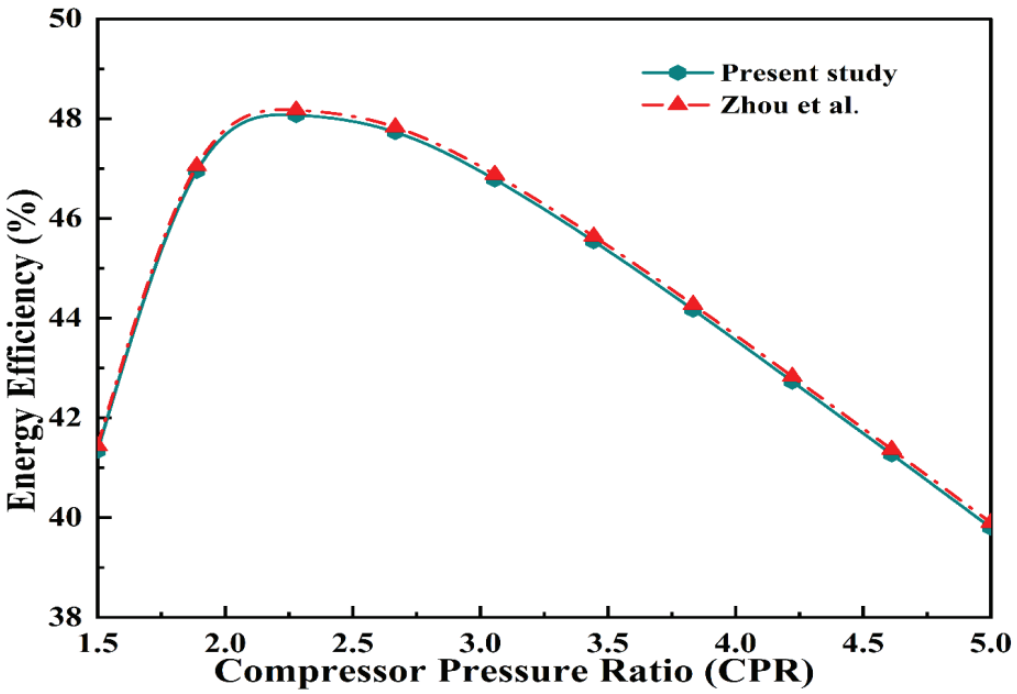

Figure 2. Validation of results of HBC.

Table 3. ORC-ERS Validation

Parameters	Present study	Dai et al. [35]	Deviation (%)
h_9	477.70	474.2	0.73
h_{10}	451.40	451	0.08
h_{11}	447.12	445.4	0.38
h_{12}	221.20	220.1	0.49
h_{13}	220.90	220.1	0.36
h_{14}	376.54	375.5	0.27
h_8	220.97	220.8	0.07
Q_E	60.70	60.4	0.49
$\dot{m}_c$	5.39	5.310	1.5
$\dot{m}_e$	0.391	0.389	0.51
$\dot{W}_{net}$	111.20	110.7	0.004

RESULTS AND DISCUSSION

Results at Initial Conditions

In this section the results of the proposed system were obtained at the base case. The thermodynamic properties at the state have been calculated by the inbuilt libraries of the EES software and listed in Table 4. However, the results at initial conditions are given in Table 5. The 14,998 kW of power was produced by the overall power plant with 23.30% of overall energy efficiency. Most of the energy (22,989 kW, or 35.72% of the total solar heat) is lost in the heliostat field, highlighting the significance of the heliostat field's design in SPT systems. While the output in terms of net power output was about 13365 kW, the standalone HBC received the heat from the IHE at a rate of about 31027 kW. Its energy efficiency was obtained as 43.07% at given operating conditions. Apart from this, the standalone ORC-ERS system obtained its energy conversion efficiency as 12.26%. It is absorbed by the 13261 kW of heat through the WHRU in terms of waste heat of topping HBC. A portion of the energy is converted into practical output for building purposes, such as electricity (1567.23 kW) through the organic turbine, heating effect (60.5 kW) through the condenser, and cooling effect (8.25 kW). Table 5 shows that the combined system (HBC-ORC-ERS) has a relatively high energy efficiency (51.68%).

Table 4. Thermodynamic properties at each state

State	Working Fluid	Pressure (kPa)	Temperature (°C)	Enthalpy (kJ/kg)	Entropy (kJ/kg·°C)	Exergy (kW)
1	Helium	2500	30	34.04	-6.569	39428
2	Helium	6250	180.8	828.6	-6.373	53992
3	Helium	6188	511	2541	-3.517	71033
4	Helium	6064	850	4301	-1.61	94593
5	Helium	2577	547.4	2720	-1.463	62455
6	Helium	2551	217.5	1007	-4112	44189
7	Helium	2525	103.8	417.2	-5.459	40460
8	Isopentane	3000	93.8	-179.5	-1.192	556.5
9	Isopentane	3000	197.5	281.7	-0.1157	4111
10	Isopentane	1500	172.1	259.6	-0.1069	3484
11	Isopentane	600	162.1	257.5	-0.01964	4622
12	Isopentane	600	50	85.9	-0.197	725.8
13	Isopentane	600	10	-15.87	-1.197	435.5
14	Isopentane	600	10	-15.87	-1.197	290.3
15	Water	100	25	104.90	0.36	0
16	Water	100	30	125.80	0.45	35.98
17	Air	101.3	561	859.9	6.763	12939
18	Air	101.3	1125	1513	7.359	38283

Table 5. Results obtained from exergy-energy evaluation*

Subsystems	Energy analysis results				Exergy analysis results			
	Input (kW)	Output (kW)	Loss (kW)	Energy efficiency	Input (kW)	Output (kW)	Destruction (kW)	Exergy efficiency
Heliostat field	64358	41369	22989	64.26%	60094	38628	21465	64.27%
Solar receiver	41369	31027	10342	75%	38628	22515	16113	58.28%
HBC	31027	13365	17662	43.07%	22515	13365	9150	59.36%
ORC-ERS	13261	1633	11634	12.26%	3729	1736	1993	46.55%
HBC-ORC-ERS	31027	14998	16035	48.33%	22515	15101	8014	64.40%
Overall plant	64358	14998	49366	23.30%	60094	15101	45593	25.12%

*T_4= 800°C, CPR=2.3, *T_8 = 197.5°C, DNI=850W/m^2;

As the results of the exergy analysis show, there is a significant irreversibility was found in SPT system since solar radiation is an excellent energy source with a heat source that is extremely hot, approximately 4500 K and receiver absorbed the heat at 1000 °C of temperature. The heliostat field has highest exergy destruction among the other components [16, 20]. The heliostat's energy efficiency was observed to be 64.27%. The absence of combustion, the primary factor contributing to irreversibility in conventional power systems, means that there is no appreciable temperature differential between the helium and HTF in the IHE. As a result, the combined cycle (HBC-ORC-ERS) has a high exergy efficiency of 64.4%. However, because of the substantial exergy destruction in the heliostat field and receiver, the power the plant's overall exergy efficiency is quite poor. The highest exergy destruction was in the heliostats and the lowest in the expansion valve, having values of 21465 kW (47.52% of total exergy destruction) and 102.5 kW, respectively. The helium turbine has the highest energy efficiency (97.25%) out of all the components. Around 59.36% was the energy efficiency determined by the solo HBC. The ORC-ERS cogeneration system achieved an energy efficiency of around 46.55%. It was determined that the ORC-ERS's addition of extra components was the cause of the decreased energy efficiency. The trigeneration system run by the SPT plant was determined to have a plant energy destruction of 45593 kW. Nonetheless, this plant achieved an energy efficiency of roughly 25.12%.

Apart from exergy, energy evaluation of the values of the exergo-environmental performance parameters at the base case has been listed in Table 6. It was seen that the exergoenvironmental impact coefficient has a large value (4.028) due to the lower exergy efficiency of the plant. It

Table 6. Values of the exergo-environmental performance parameters at base case

Parameters	Values
Exergoenvironmental impact factor (f_{ei})	0.7517
Exergoenvironmental impact coefficient (C_{ei})	4.028
Exergoenvironmental impact index (θ_{ei})	3.028
Exergy stability factor (f_{es})	0.2483
Exergoenvironmental impact improvement (θ_{eii})	0.3302
Exergetic sustainability index (θ_{est})	0.0819

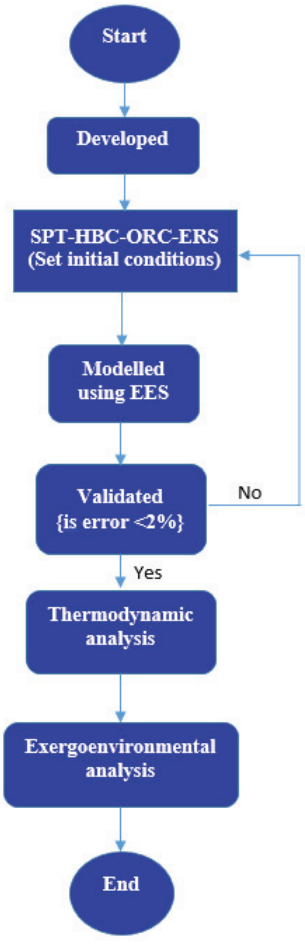

Figure 3. Flowchart of step-by-step methods during simulations.

revealed that there is still much scope to reduce the environmental effects. The exergetic stability factor should be one. However, it was found to be 0.2483; it means still this system affected the environment from a stability point of view. To enhance the exergetic stability of the system and move closer to the ideal value of 1, the following action can be considered: Optimize components such as the combustion chamber, heat exchangers, and turbines to reduce internal irreversibilities.

Parametric Analysis

The trigeneration plant's performance was evaluated by varying the compressor pressure ratio (CPR). With increasing CPR, both energy and exergy efficiency initially improved, reaching a peak at 2.3 CPR, before steadily declining, as depicted in Figure 4(a). This decline commences after reaching a CPR of 2.3. This trend can be rationalized by considering the enhanced expansion and compression works before reaching a CPR of 2.3. However, in this context, the rate of improvement in compression work is lower than that of expansion work. Consequently, the network output increases, leading to improvements in both efficiencies of the plant. Subsequent to a CPR of 2.3, the results demonstrated a reverse trend. The combined ORC-ERS system achieved peak energy and exergy efficiencies of 48.33% and 64.40%, respectively, whereas the overall plant achieved values around 23.3% and 25.12%, respectively. Although the cycle may have experienced considerable energy loss, the loss is minimal due to the poor quality of the lost energy, explaining the discrepancy in energy and energy efficiency of the cycle. In the solar field alone, heliostats and receivers accounted for 83.20% of the total energy loss, indicating that 45593 kW of plant energy was lost overall, with only 37578 kW of solar field energy being lost. The highest power from the HBC and the plant were found to be 14998 kW and 13365 kW, respectively, at a CPR of 2.3, which is the optimal value. Consequently, there was an improvement of 1633 kW in net power output due to the ORC-ERS. At a CPR of 2.3, the greatest cooling and heating impacts were measured at 8.82 kW and 60.56 kW, respectively. The power output, energy, and energy conversion efficiency all follow the same trend.

The inlet temperature of the helium turbine (HTIT) plays a significant role in influencing the system's performance. As depicted in Figure 4(b), the plant's energy efficiency, exergy efficiency, and power production improved from 21.36% to 24.65%, 23.87% to 27.4%, and 13808 kW to 15928 kW, respectively, with HTIT. This can be attributed to the increase in enthalpy differential across the turbine as the input temperature rises. Consequently, there is a rise in net expansion effort, leading to enhancements in net output power and the thermodynamic performance of the system. This change was assessed under conditions of 197.5°C for the OT inlet temperature, 850 W/m² of DNI, and an optimal CPR of 2.3. Furthermore, the HTIT affects the cooling and heating impacts in addition to efficiency and net power output. The effects of heating and cooling were enhanced with a rise in HTIT. As the HTIT enhanced from 700°C to 900°C, the cooling load increased from 6.87 kW to 10.40 kW, and the heating load climbed from 55.87 kW to 59.4 kW. This relationship makes sense because rising HTIT and ORC turbine input temperatures indicate more heat energy entering the ORC-ERS system and amplifying the impacts of heating and cooling.

The system's performance declined with the compressor inlet temperature (CIT). This can be explained by the fact that as CIT increased, the enthalpy differential within the compressor itself also increased, resulting in an enhancement in compressor work. Consequently, CIT reduced the overall performance of the system. The facility's overall energy and exergy efficiency decreased from 23.36% to 23% and from 26.02% to 25.63%, respectively. As depicted in Figure 4(c), the power output decreased from 15034 kW to 14802 kW with said CIT. The loads for heating and cooling remained unaffected by CIT. The net work production from the ORC declined as CIT increased, indicating that the output heat had minimal effect on the slight change in condenser and evaporator loads.

The pump pressure ratio (PPR) plays a significant role in influencing the performance of the system. By maintaining a constant value of 2.3 for the CPR, 850 W/m² for DNI, and 800°C for T_4, the variation in thermal performance was examined. The overall efficiencies of the plant initially increased and then exhibited a continuous decrease, reaching an optimal value where the system's performance was maximized. As illustrated in Figure 4(d), the highest energy efficiency and exergy efficiency for the entire plant were achieved at the optimal PPR of 3.056, amounting to 25.12% and 23.30%, respectively. Notably, the cooling aspect remained unaffected by changes in PPR, while the heating effects demonstrated a consistent increase with higher PPR values. An increase in PPR implies more work for the pump resulting in no enhancement in refrigeration effects. However, an increase in PPR leads to greater heat extraction through the condenser to maintain energy balance, necessitating increased heat rejection through the condenser, thereby augmenting the heating load. Specifically, a 2.33% increase in PPR resulted in a 6.31% increase in heating effects.

Figure 5(a) depicts the variation in the system's performance with changes in the evaporator temperature. Understanding the impact of the evaporator on the trigeneration system's performance is crucial in any cooling setup. As the evaporator temperature increases, there is a consistent improvement in both energy and exergy efficiency, along with an increase in the power output of the energy conversion system. Specifically, the output power rose from 15802 kW to 16034 kW, while the energy and exergy efficiency increased from 22.85% to 23.32% and 24.48% to 24.92%, respectively. The evaporator temperature has no discernible effect on the heating loads but significantly

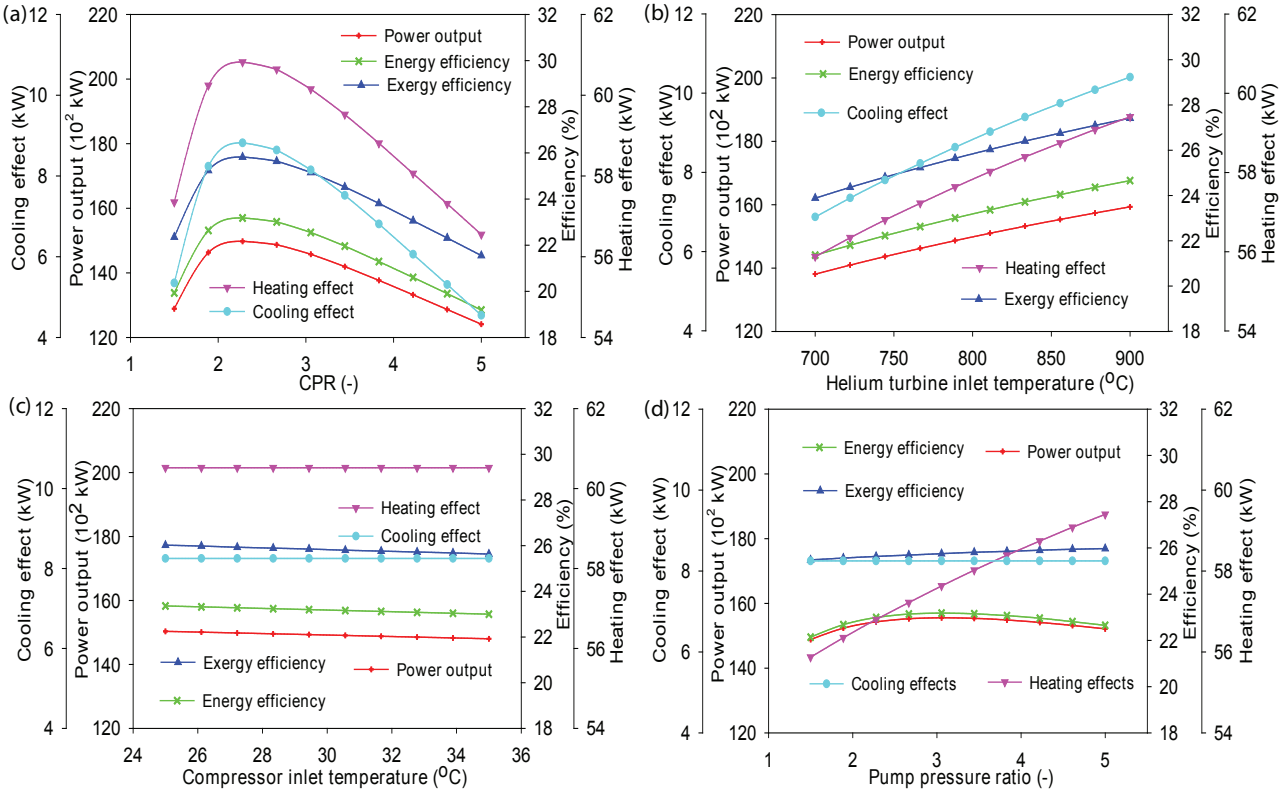

Figure 4. Performance variation with (a) CPR, (b) HTIT, (c) CIT, (d) PPR.

influences the cooling load. It's established that the evaporator temperature does not impact the thermodynamic parameters of the condenser, by elevating the evaporator pressure, thereby enhancing the cooling loads.

Figure 5(b) also demonstrates an increase in power output with Direct Normal Irradiance (DNI). In Indian climate conditions, the average DNI was determined to be 850 W/m². With higher DNI values, the receiver efficiency is expected to rise, consequently enhancing the energy performance of the plant. As DNI levels rose from 600 W/m² to 1000 W/m², Figure 5 illustrates the variations in energy efficiency, power output, and energy efficiency, ranging from 22.87% to 26.4%, 21.36% to 24.65%, and 13808 kW to 15928 kW, respectively. Furthermore, both cooling and heating loads rise with Direct Normal Irradiance (DNI). The uptick in DNI provides extra energy to the cycle, resulting in a greater amount of energy being converted into useful output, thereby leading to increased heating and cooling loads. As Figure 6 shows, for example, the heating and cooling loads went from 55.98 kW to 59.6 kW and from 6.87 kW to 9.99 kW, respectively, while the DNI increased from 600 W/m² to 1000 W/m².

Figure 5(c) emphasizes the significance of discussing the design parameters of the Solar Power Tower (SPT) alongside the combined cycle parameters. Among these, the heliostat field efficiency stands out as a key factor impacting the plant's performance. As the efficiency of the heliostat field increases, the overall performance of the plant improves. The energy efficiency, power generation, and output exertion are shown in Figure 5(c) as they increase from 21.19% to 30.83%, 19.64% to 28.65%, and 13925 kW to 19728 kW, respectively, while the heliostat efficiency rises from 0.6 to 0.85. This development is ascribed to the reduced solar energy loss brought about by increased heliostat efficiency, which results in more effective power conversion. As a result, improvements in power, energy, and exergy were noted. Furthermore, when field efficiency grew, so did the cooling and heating loads. With the heliostat efficiency increasing from 0.6 to 0.85, the cooling and heat demand grew by 51.38% and 6.31%, respectively.

Effects of various parameters on exergoenvironmental performance

Exergo-environmental analysis is an approach used in the study of thermodynamics and sustainability to evaluate and examine how energy systems and processes affect the environment. Figure 6(a) depicts the impact of compressor pressure ratio on exergo-environmental factors. It is evident from the figure that, as CPR increases, the environmental impact index (θ_{ei}) decreases and reaches a minimum value of 3 at a pressure ratio of 2.33. Subsequently, it gradually increases with further pressure ratio increments. This phenomenon arises due to lower exergy destruction at lower pressure ratios, which becomes more pronounced at higher

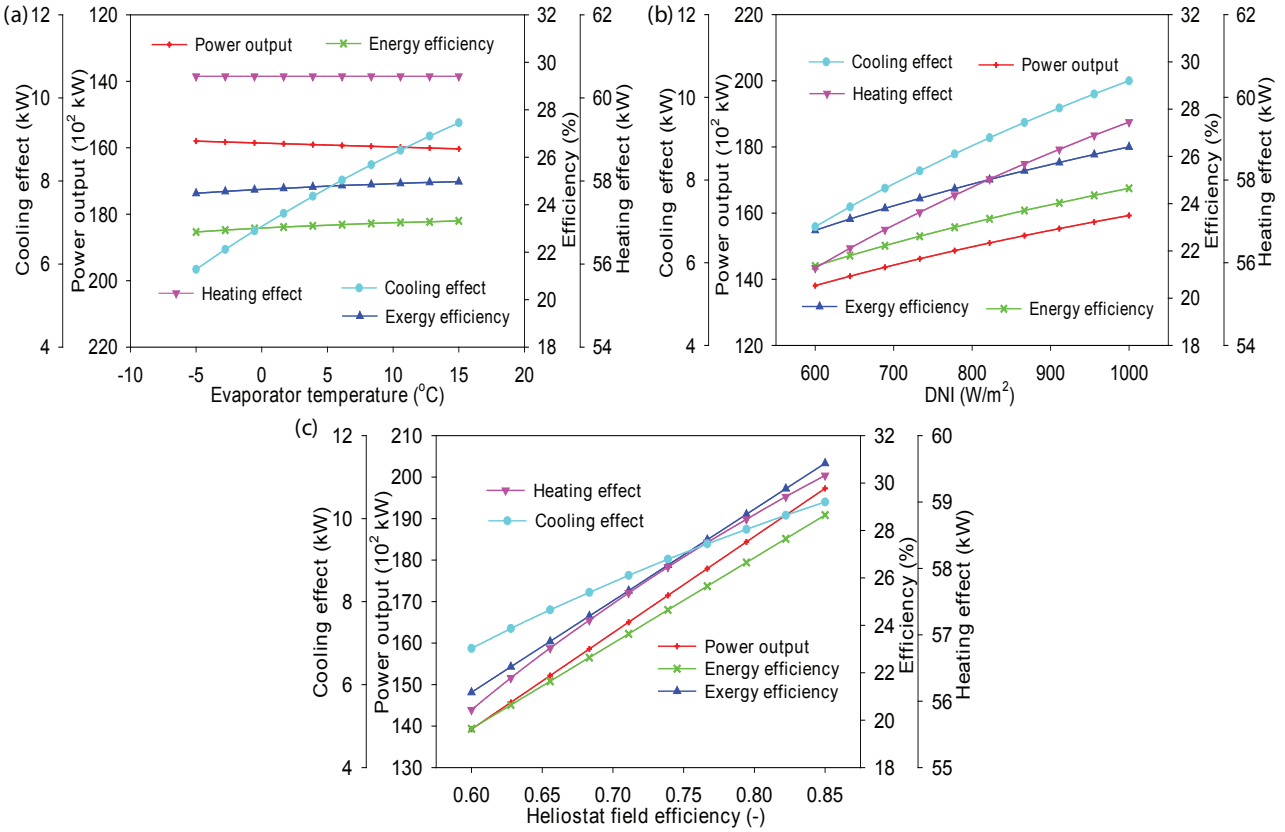

Figure 5. Performance variation with (a) evaporator temperature, (b) DNI, (c) heliostats field efficiency.

pressure ratios. Similarly, other environmental factors such as the environmental impact factor (θ_{eii}), exergy sustainability index (θ_{est}), and exergy stability factor (f_{es}) exhibit a similar trend. Exergy efficiency increases with pressure ratio up to 2.3 and then declines as pressure ratio continues to rise. In the graph, θ_{ei} decreases from 3.68 to 3 of CPR 2.33 and then increases to 3.8 at a CPR of 5. The factors θ_{eii}, θ_{est}, and f_{es} increases from 0.27 to 0.32, 0.05 to 0.07, and 0.21 to 0.24, respectively, as CPR increases from 1.5 to 2.33, reaching their maximum values at 2.33 and subsequently decreasing with further pressure ratio increases.

Figure 6(b) illustrates the impact of HT inlet temperature on exergo-environmental factors. It is seen that, as the HTIT incresed, θ_{ei} decreases, whereas the other factors, namely θ_{eii}, θ_{est}, and f_{es}, increases with the rising HTIT. This trend is a result of the minimum exergy destruction at lower temperatures, while higher temperatures lead to increased exergy destruction. The θ_{ei} decreases from 3.37 to 2.78, while the factors θ_{ei}, θ_{est}, and f_{es} increases from 0.29 to 0.35, 0.06 to 0.09, and 0.2 to 0.26, respectively, as the temperature increases from 700°C to 900°C.

Figure 6(c) illustrates the relationship between heliostat field efficiency and exergo-environmental factors. As observed in the graph, θ_{ei} decreases, while the other factors, including θ_{eii}, θ_{est}, and f_{es}, increase as heliostat field efficiency rises from 50% to 90%. The value of θ_{ei} decreases from 4.17 to 1.8, while the factors θ_{eii}, θ_{est}, and f_{es} increase from 0.23 to 0.53, 0.04 to 0.18, and 0.19 to 0.34, respectively. This trend emerges because the heliostat field receives the maximum amount of solar energy, with temperatures around 2000 °C. Consequently, such high temperatures result in maximum exergy destruction within the heliostat field. Therefore, it can be concluded that the present study has negligible harmful impact on the environment and thus power is generated in a green manner.

Comparative Study

According to published research, the SPT plant components have undergone a number of irreversibilities that are unavoidable. Consequently, the implementation of an efficient power generation system is necessary to enhance the overall performance of the SPT plant. The performance of the novel SPT-based integrated system is compared with earlier systems developed by other authors in this field. For a real comparison, the same solar circumstances are employed, and Table 12 lists the outcomes. The findings show that the combined system in present work performs better than previous comparable systems. This is due to the advanced cycle configuration and effective utilization of the waste heat from the topping cycle as compared to the Rankine cycle and sCO_2 cycle. It is evident from Table

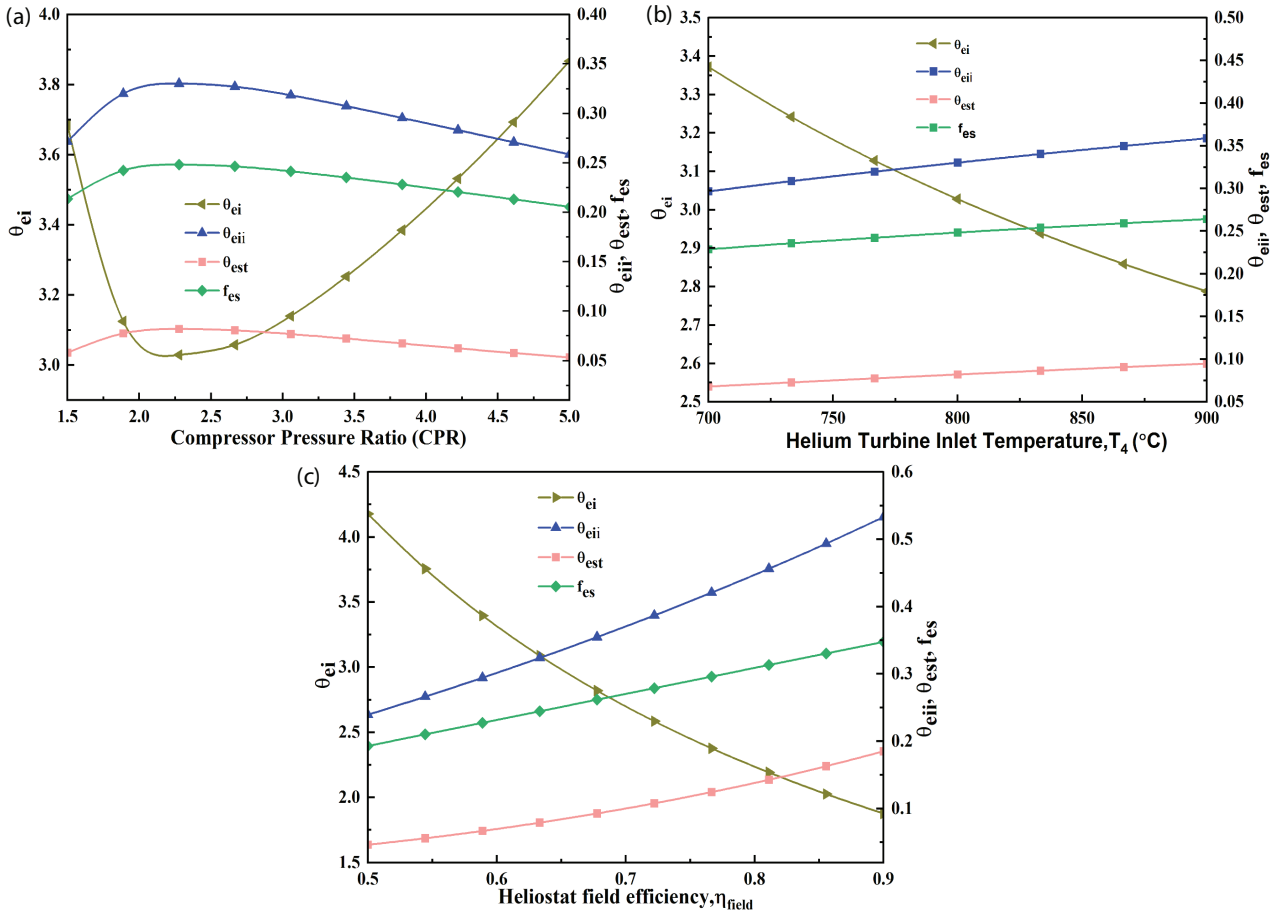

Figure 6. Exergoenvironmental performance variation with (a) CPR, (b) HTIT, (c) heliostats field efficiency.

Table 7. Comparison of the findings with related earlier research

Systems	DNI (kW/m²)	η_{field}	$\eta_{field} \times \eta_{rec}$	η_{rec}	$\eta_{en.comb}$ (%)	$\eta_{en.Plant}$ (%)	$\eta_{ex.Plant}$ (%)
Regenerative Rankine cycle [36]	0.8	0.75	-	0.9	37.9	22.9	24.5
Present system	0.8	0.75	-	0.9	56.67	38.02	41.15
Supercritical CO_2 cycle [36]	1	-	0.62	-	42.48	26.23	28.14
Present system	1	-	0.62	-	57.97	38.89	41.86

7 that the proposed SPT-HBC-ORC-ERS system, which is modelled in this work, obtained 48.75%, and 67.95% higher exergy efficiency than that of the combined HBC-basic ORC, sCO_2 system, and SPT-based Rankine cycle, respectively.

CONCLUSION

In this study, a trigeneration system has been developed to concurrently provide cooling, heating, and power for building applications like hospitals and hostels, utilizing a solar power tower (SPT). Power generation is achieved through a HBC and an ORC turbine, while ejector refrigeration has been integrated for cooling purposes. Heat rejected through the condenser is utilized for heating. The study's findings led to the following conclusions:

- The HBC-ORC-ERS system demonstrated exergy and energy efficiencies of 64.4%, and 48.33%, respectively, at a compression pressure ratio of 2.3 and a direct normal irradiance of 850 W/m².
- The overall plant (SPT-HBC-ORC-ERS) achieved an exergy efficiency of 25.12%, an energy efficiency of 23.3%, and a power output of 14998 kW. Therefore, considering the SPT performance overall performance

is reduced. It shows the greater irreversibility is associated with the SPT system. Additionally, heating and cooling loads were recorded at 60.52 kW and 8.25 kW, respectively.
- The highest exergy destruction rate was observed in the solar power tower subsystem (receiver and heliostats), accounting for approximately 83.20% (37,578 kW) of the total exergy destruction (45,593 kW) of the overall plant.
- It was seen that the exergoenvironmental impact coefficient has large value (4.028) due to the lower exergy efficiency of the plant. It revealed that still much scope is there to reduce the environmental effects.
- The exergetic stability factor was found as 0.2483. However, it's value close to one is preferable for power plant.

Limitations and Future Scope
- This study is limited to the thermodynamic and environmental analysis. Also this study provides the power at the peak load conditions only due to absence of the energy storage system.
- Exergoeconomic analysis and the analysis with energy storage are the future scope of this work.

NOMENCLATURE

A	Area (m^2)
$\dot{m}$	Mass flow rate (kg/s)
$\dot{E}X$	Rate of exergy (kW)
$\dot{Q}$	Heat rate (kW)
s	Specific entropy (kJ/kg·K)
T	Temperature (K)
h	Specific enthalpy (kJ/kg)
$\dot{E}D$	Exergy destruction rate (kW)
N_{hel}	Number of heliostats
$\dot{W}$	Power (kW)

Abbreviations

CIT	Compressor inlet temperature
HC	Helium compressor
DNI	Direct normal irradiation
CPR	Compressor pressure ratio
HTIT	Helium turbine inlet temperature
ORC	Organic Rankine cycle
HBC	Helium Brayton cycle
IHE	Intermediate heat exchanger
HT	Helium turbine
sCO_2	SupercriticalCO_2
tCO_2	Transcritical CO_2
WHRU	Waste heat recovery unit
PPR	Pump pressure ratio
SPT	Solar power tower

Subscripts

E	Evaporator
C	Condenser
P	Pump
e	exit
0	dead condition
j	particular state
ref	reference/reflectivity
rec	receiver
i	inlet
hel	heliostat
en	Energy
ex	Exergy

Greek letters

η	Efficiency
ε	Effectiveness
μ	Entertainment ratio

AUTHORSHIP CONTRIBUTIONS

Authors equally contributed to this work.

DATA AVAILABILITY STATEMENT

The authors confirm that the data that supports the findings of this study are available within the article. Raw data that support the finding of this study are available from the corresponding author, upon reasonable request.

CONFLICT OF INTEREST

The author declared no potential conflicts of interest with respect to the research, authorship, and/or publication of this article.

ETHICS

There are no ethical issues with the publication of this manuscript.

STATEMENT ON THE USE OF ARTIFICIAL INTELLIGENCE

Artificial intelligence was not used in the preparation of the article.

REFERENCES

[1] Khan Y, Tevatia A, Apparao D, et al. Experimental investigation to evaluate thermal performance of a solar cooker with evacuated tube solar collector using different heat transfer fluids. J Therm Eng 2024;10:1346−1357. [CrossRef]

[2] Khan Y, Raman R, Rashidi MM, et al. Thermodynamic analysis and experimental investigation of the water spray cooling of photovoltaic solar panels. J Therm Anal Calorim 2024;149:2073−2086.

[3] Khan Y, Mishra RS. Thermo-economic analysis of the combined solar-based pre-compression supercritical CO2 cycle and organic Rankine cycle using ultra-low GWP fluids. Therm Sci Eng Prog 2021;23:100925. [CrossRef]
[4] Chauhan MK, Chauhan AK, Khan Y, et al. Experimental and theoretical investigation of thermal efficiency and productivity of single slope basin type solar distillation system using honey-comb. J Therm Eng 2023;9:1559−1571. [CrossRef]
[5] Khan Y, Mishra RS, Singh AP. Performance comparison of organic Rankine cycles integrated with solar based combined cycle: A thermodynamic and exergoenvironmental analysis. Proc Inst Mech Eng Part C J Mech Eng Sci 2024;238:233−248. [CrossRef]
[6] Pal JS, Sapali SN, Deshmukh PW. Estimation and analysis of exergy loss and performance evaluation of marine freshwater generating system. J Therm Eng 2024;10:1266−1274. [CrossRef]
[7] Bader NM, Mushatet KS. An experimental study for a single-pass solar air heater integrated with artificial roughness. J Therm Eng 2024;10:1292−1305. [CrossRef]
[8] Kushwah A, Kumar A, Gaur MK. Techno-economic analysis of solar still with nano-phase change material and heating coil: A novel approach for sustainable development. J Therm Eng 2025;11:476−492. [CrossRef]
[9] Khan Y, Mishra RS. Performance analysis of a solar based novel trigeneration system using cascaded vapor absorption-compression refrigeration system. Int J Refrig 2023;155:207−218. [CrossRef]
[10] Guo J, Li M, He Y, Wang Y, Gong L. A systematic review of supercritical carbon dioxide (S-CO2) power cycle for energy industries: Technologies, key issues, and potential prospects. Energy Convers Manag 2022;258:115437. [CrossRef]
[11] Gkountas AA, Benos LT, Nikas KS, Sarris IE. Heat transfer improvement by an Al2O3-water nanofluid coolant in printed-circuit heat exchangers of supercritical CO2 Brayton cycle. Therm Sci Eng Prog 2020;20:100694. [CrossRef]
[12] Chai L, Tassou SA. A review of printed circuit heat exchangers for helium and supercritical CO2 Brayton cycles. Therm Sci Eng Prog 2020;18:100543. [CrossRef]
[13] Qin L, Xie G, Ma Y, Zhang S. Thermodynamic analysis and multi-objective optimization of a waste heat recovery system with a combined supercritical/transcritical CO2 cycle. Energy 2023;265:126332. [CrossRef]
[14] Khatoon S, Kim M. Preliminary design and assessment of concentrated solar power plant using supercritical carbon dioxide Brayton cycles. Energy Convers Manag 2022;252:115066. [CrossRef]
[15] Khan Y, Mishra RS. Performance analysis of solar driven combined recompression main compressor intercooling supercritical CO2 cycle and organic Rankine cycle using low GWP fluids. Energy Built Environ 2022;3:496−507. [CrossRef]
[16] Zare V, Hasanzadeh M. Energy and exergy analysis of a closed Brayton cycle-based combined cycle for solar power tower plants. Energy Convers Manag 2016;128:227−237. [CrossRef]
[17] Khan Y, Singh D, Caliskan H, Mishra RS. Exergoeconomic and thermodynamic analyses of solar power tower based novel combined helium Brayton cycle-transcritical CO2 cycle for carbon free power generation. Glob Chall 2023;7:2300191. [CrossRef]
[18] Bi Y, Ju Y. Design and analysis of an efficient hydrogen liquefaction process based on helium reverse Brayton cycle integrating with steam methane reforming and liquefied natural gas cold energy utilization. Energy 2022;252:124047. [CrossRef]
[19] Li Q, Wang E, Qiu Y. Triple-objective optimization of He Brayton cycles for ultra-high-temperature solar power tower. Energy Convers Manag 2022;270:116210. [CrossRef]
[20] Zhou J, Ali MA, Zeki FM, et al. Thermoeconomic investigation and multi-objective optimization of a novel efficient solar tower power plant based on supercritical Brayton cycle with inlet cooling. Therm Sci Eng Prog 2023;39:101679. [CrossRef]
[21] Wang M, Wang J, Zhao P, Dai Y. Multi-objective optimization of a combined cooling, heating and power system driven by solar energy. Energy Convers Manag 2015;89:289−297. [CrossRef]
[22] Mishra SK, Rehalia AS, Verma AK, Yadav L. Thermo-economic analysis of solar-powered trigeneration system with integrated ejector-absorption recompression and modified organic Rankine cycle. J Eng Gas Turbines Power 2024;146:051024. [CrossRef]
[23] Ogaili HH, Khalilarya S, Chitsaz A, Mojaver P. Energy, exergy, and economic performance analysis of integrated parabolic trough collector with organic Rankine cycle and ejector refrigeration cycle. Energy Convers Manag X 2025;25:100843. [CrossRef]
[24] Saladi JK, Suresh R, Datta SP. Diurnal performance investigation of solar integrated ejector-based combined cooling, heating, and power (CCHP) system for Indian climate. Appl Therm Eng 2025;263:125250. [CrossRef]
[25] Khan Y, Mishra RS. Performance evaluation of solar based combined pre-compression supercritical CO2 cycle and organic Rankine cycle. Int J Green Energy 2021;18:172−186. [CrossRef]
[26] Khan Y, Mishra RS. Parametric (exergy-energy) analysis of parabolic trough solar collector-driven combined partial heating supercritical CO2 cycle and organic Rankine cycle. Energy Sources Part A Recovery Util Environ Eff 2023;45:6019−6039.

[27] Li M, Wang J, He W, Gao L, Wang B, Ma S, et al. Construction and preliminary test of a low-temperature regenerative organic Rankine cycle (ORC) using R123. Renew Energy 2013;57:216–222. [CrossRef]
[28] Olumayegun O, Wang M, Kelsall G. Closed-cycle gas turbine for power generation: a state-of-the-art review. Fuel 2016;180:694–717. [CrossRef]
[29] Dunham MT, Iverson BD. High-efficiency thermodynamic power cycles for concentrated solar power systems. Renew Sustain Energy Rev 2014;30:758–770. [CrossRef]
[30] Xu C, Wang Z, Li X, Sun F. Energy and exergy analysis of solar power tower plants. Appl Therm Eng 2011;31:3904–3913. [CrossRef]
[31] Bellos E, Tzivanidis C. Multi-objective optimization of a solar driven trigeneration system. Energy 2018;149:47–62. [CrossRef]
[32] Li H, Cao F, Bu X, Wang L, Wang X. Performance characteristics of R1234yf ejector-expansion refrigeration cycle. Appl Energy 2014;121:96–103. [CrossRef]
[33] Wang J, Dai Y, Sun Z. A theoretical study on a novel combined power and ejector refrigeration cycle. Int J Refrig 2009;32:1186–1194. [CrossRef]
[34] Zare V, Mahmoudi SMS, Yari M. On the exergoeconomic assessment of employing Kalina cycle for GT-MHR waste heat utilization. Energy Convers Manag 2015;90:364–374. [CrossRef]
[35] Dai Y, Wang J, Gao L. Exergy analysis, parametric analysis and optimization for a novel combined power and ejector refrigeration cycle. Appl Therm Eng 2009;29:1983–1990. [CrossRef]
[36] Chacartegui R, Muñoz de Escalona JM, Sánchez D. Alternative cycles based on carbon dioxide for central receiver solar power plants. Appl Therm Eng 2011;31:872–879. [CrossRef]